Digital Twin-Based Research on Fiber Optic Current Sensor Behavior and Stability

Valentina Temkina(✉), Andrei Medvedev, and Alexey Mayzel

Peter the Great St. Petersburg Polytechnic University (SPbPU), Polytechnicheskaya, 29, St. Petersburg 195251, Russia
temkina.vs@edu.spbstu.ru, medvedev@rphf.spbstu.ru, amayzel@gmail.com

Abstract. Digital Twin technology as an idea of implementing simulation models of particularly every physical entity became universally adopted in the last five years thanks to a huge leap in computer hardware performance and software tools evolution. The early pioneers of Fiber Optic Current Sensors (FOCS) technology in the late 90-th had no access to such an advanced research tool as digital twin of the product being developed. As a result, nowadays FOCS remain undervalued due to its legacy problems including the lack of stability and high cost. However, the Connected World, Industrial Internet of Things open the great opportunities for new metering technologies in power grid. The modern computer simulation approaches helped us in this challenge to bypass the caveats of FOCS, to understand and improve this technology making it more accurate, robust and more competitive in its field.

Keywords: Fiber-Optic Current Sensor · Faraday Effect · Digital twin · Computer simulation · LabVIEW FPGA

1 Introduction

The fourth industrial revolution aims to higher the efficiency of every production by increasing the transparency of every facility and process. Basically, this means first acquiring multiple measurements at every step in the digital form. In power grid, this tendency is implemented with replacing legacy analog voltage and current sensors with digital devices and an ecosystem commonly called Digital Substation technology. These digital measurement devices could be both traditional measuring transformers with analog-to-digital converters (ADCs) or implement other physical phenomena not suited in analog era.

Due to the active introduction of digital substations and the development of Smart Grids in the energy sector, optical current transformers have been developed for several decades [1–3]. This technology has a number of advantages over its inductive analog (electromagnetic current transformers), one of the main of which is the fully dielectric structure of the device measuring part, located in the high voltage region. However, despite all the success of developers of optical current transformers, their application in

O. Galinina et al. (Eds.): NEW2AN 2020/ruSMART 2020, LNCS 12526, pp. 373–383, 2020.
https://doi.org/10.1007/978-3-030-65729-1_33

electrical substations is still limited due to insufficient accuracy, measurement instability and high cost of construction.

Optical transformers that operate basing on the Faraday Effect in a special optical waveguide are being developed to measure the amplitude and spectral distribution of the industrial frequency current in electric networks of 110–220 kV and higher [4–7]. The sensing element of such meter is a spun fiber wrapped around a current conductor. The phase difference between the two circularly polarized light modes is induced in the sensitive fiber under the action of the magnetic field produced by the measured current.

To satisfy the industry demand the FOCS must meet the accuracy class 0.2 and convert the measured values into a digital data stream in accordance with the IEC 61850-9-2 (2011) standard. Therefore, the task of improving the accuracy and stability of such devices is relevant.

We have built the laboratory prototype of the FOCS based on a well-known optical scheme, which is described and studied in detail in [8]. The meter used additional phase modulation by a harmonic signal and digital phase detection based on the ratio analysis of modulation frequency harmonics. We used LabVIEW FPGA and National Instruments hardware platform to rapidly implement control and demodulation functionality into the mock-up. In addition, we have conducted a number of researches of the FOCS laboratory prototype to improve the accuracy and stability of measurements, as well as reduce the cost of the device [8, 9]. Our research demonstrated that the meter measurement accuracy was influenced by a set of external factors, and it was difficult to study the system response to each factor individually in the real prototype. In turn, a computer model of the FOCS will allow us to study the influence of many parasitic factors separately, as well as to check-out the signal processing algorithms, which is also necessary to provide real time high-precision measurements.

2 Modeling Method of the Fiber Optic Current Sensor

Modeling of the FOCS was based on the formalism of Jones matrices. According to this method, each element of the optical circuit can be represented by a 2×2 matrix describing the transformation of the polarization state of light when passing through this element. The optical scheme of the FOCS is shown in Fig. 1.

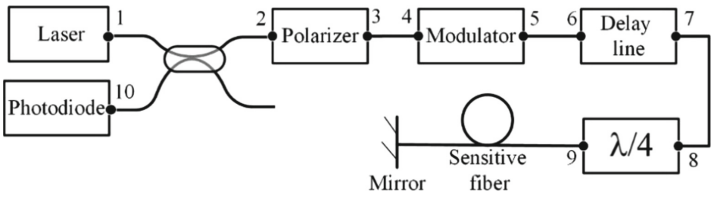

Fig. 1. Optical scheme of the FOCS. The numbers 1–10 indicate the junctions between optical elements or fiber splicing.

The modulator and the quarter-wave plate can be represented by matrices of phase plates in the basis of linear polarizations according the Eq. (1)

$$[K_n] = [K(\varphi_n)] = \begin{bmatrix} e^{-j\varphi_n/2} & 0 \\ 0 & e^{j\varphi_n/2} \end{bmatrix}, \tag{1}$$

where φ_n is the phase difference between the polarization modes formed during propagation through the element. Phase plate matrices for different elements have the same structure, but differ in phases. In the modulator, the phase shift consists of two terms according to the Eq. (2). The first random slowly changing value φ^0_{mod} represents the quasi-static phase difference between the two polarization modes, and the second is variable and is determined by the modulating signal $U_{\text{mod}}(t)$

$$\varphi_{\text{mod}} = \varphi^0_{\text{mod}} + k_U U_{\text{mod}}(t). \tag{2}$$

The quarter-wave plate introduces a phase difference between the two polarization components equal to

$$\varphi_{\lambda/4} = \frac{\pi}{2} + \pi m, \tag{3}$$

where m is an integer.

Rotation matrices were introduced to account for the rotation of coordinate axes to any element of the optical scheme relative to another element or relative chosen basis according Eq. (4)

$$[R_n] = [R(\alpha_n)] = \begin{bmatrix} \cos\alpha_n & -\sin\alpha_n \\ \sin\alpha_n & \cos\alpha_n \end{bmatrix}, \tag{4}$$

where α_n are the angles at the points where the fibers connect to each other or to elements. It should be noted that in the basis of linear polarizations, the sensitive fiber is also described by a rotation matrix. Since the plane of linear polarization of light turns at an angle $\varphi_F/2$ proportional to the current due to the Faraday Effect, which is identical to the change on φ_F in the phase difference between light modes of circular polarization.

A polarizer transmits only one polarization, which coincides with its own axis and in the ideal case, the matrix of the polarizer has the following form

$$[P] = \begin{bmatrix} 1 & 0 \\ 0 & 0 \end{bmatrix}. \tag{5}$$

When the light falls directly on the mirror and then reflects off it, the direction of light propagation changes to the opposite. Accordingly, the mirror matrix must be such that a right-handed coordinate system is preserved. To do this, it is necessary to maintain the direction of one of the transverse axes and change the direction of the other to the opposite. Thus, the mirror matrix is a half-wave plate matrix [10]. Let the x-axis keep the direction, and y-axis changes it by 180°, then the mirror matrix can be written as

$$F_{mir} = \begin{bmatrix} 1 & 0 \\ 0 & -1 \end{bmatrix}. \tag{6}$$

In addition, when the light propagates in the opposite direction through the elements, their matrices must be modified. If the matrix of an reciprocal element in a forward direction is described by an equation

$$B = \begin{bmatrix} b_{11} & b_{12} \\ b_{21} & b_{22} \end{bmatrix}, \tag{7}$$

then in the reverse direction of light propagation through this element, its matrix will have the following form [10]

$$\overline{B} = \begin{bmatrix} b_{11} & -b_{21} \\ -b_{12} & b_{22} \end{bmatrix}. \tag{8}$$

The fiber delay line in the optical circuit of the FOCS must provide such a delay between two orthogonally polarized modes that when light propagates from the modulator to the mirror and back, the phase of the modulating voltage changes sign to the opposite. Therefore, in the case of an ideal delay line, its influence will be taken into account directly in the modulator matrices.

Thus, sequentially multiplying the matrices of each optical element in the order opposite to the direction of light propagation in the scheme, we get the common matrix of the system

$$T = \overline{R_{10}} \cdot \overline{R_2} \cdot \overline{\mathrm{P}} \cdot \overline{R_3} \cdot \overline{R_4} \cdot \overline{M} \cdot \overline{R_5} \cdot \overline{R_6} \cdot \overline{F_{dl}} \cdot \overline{R_7} \cdot \overline{R_8} \cdot \overline{F_{\lambda/4}} \cdot \overline{R_9} \cdot \overline{S} \cdot F_{mir} \cdot \mathrm{S} \cdot R_9 \cdot F_{\lambda/4} \cdot \\ \cdot R_8 \cdot R_7 \cdot F_{dl} \cdot R_6 \cdot R_5 \cdot M \cdot R_4 \cdot R_3 \cdot \mathrm{P} \cdot R_2 \cdot R_1, \tag{9}$$

wherein $[R_{1–10}]$ is the rotation matrix by angle $\alpha_{1–10}$, $[P]$ is the polarizer matrix, $[M]$ is the modulator matrix, $[F_{dl}]$ is the delay line matrix, $[F_{\lambda/4}]$ is the quarter-wave plate matrix, $[S]$ is the sensor matrix, $[F_{mir}]$ is the mirror matrix. The numbers 1–10 indicate the junction of optical elements or fiber splicing in accordance with Fig. 1.

When all the optical elements are ideal and $\alpha_1 = \alpha_2 = \alpha_4 = \alpha_5 = \alpha_6 = \alpha_7 = \alpha_{10} = 0°$, $\alpha_3 = \alpha_8 = 45°$, $\alpha_9 = -45°$, the common matrix of the system $[T]$ is determined by the following equation

$$[T] = \begin{bmatrix} 1 & 0 \\ 0 & 0 \end{bmatrix} \cdot \begin{bmatrix} \cos 45° & -\sin 45° \\ \sin 45° & \cos 45° \end{bmatrix} \cdot \begin{bmatrix} e^{\frac{1}{2}j\varphi_{\mathrm{mod}}} & 0 \\ 0 & e^{-\frac{1}{2}j\varphi_{\mathrm{mod}}} \end{bmatrix} \cdot \begin{bmatrix} \cos 45° & -\sin 45° \\ \sin 45° & \cos 45° \end{bmatrix} \cdot \\ \cdot \begin{bmatrix} e^{-\frac{j\pi}{4}} & 0 \\ 0 & e^{\frac{j\pi}{4}} \end{bmatrix} \cdot \begin{bmatrix} \cos 45° & \sin 45° \\ -\sin 45° & \cos 45° \end{bmatrix} \cdot \begin{bmatrix} \cos \frac{\varphi_F}{2} & \sin \frac{\varphi_F}{2} \\ -\sin \frac{\varphi_F}{2} & \cos \frac{\varphi_F}{2} \end{bmatrix} \cdot \begin{bmatrix} 1 & 0 \\ 0 & -1 \end{bmatrix} \cdot \\ \cdot \begin{bmatrix} \cos \frac{\varphi_F}{2} & -\sin \frac{\varphi_F}{2} \\ \sin \frac{\varphi_F}{2} & \cos \frac{\varphi_F}{2} \end{bmatrix} \cdot \begin{bmatrix} \cos 45° & \sin 45° \\ -\sin 45° & \cos 45° \end{bmatrix} \cdot \begin{bmatrix} e^{-\frac{j\pi}{4}} & 0 \\ 0 & e^{\frac{j\pi}{4}} \end{bmatrix} \cdot \\ \cdot \begin{bmatrix} \cos 45° & -\sin 45° \\ \sin 45° & \cos 45° \end{bmatrix} \cdot \begin{bmatrix} e^{-\frac{1}{2}j\varphi_{\mathrm{mod}}} & 0 \\ 0 & e^{\frac{1}{2}j\varphi_{\mathrm{mod}}} \end{bmatrix} \cdot \begin{bmatrix} \cos 45° & -\sin 45° \\ \sin 45° & \cos 45° \end{bmatrix} \cdot \begin{bmatrix} 1 & 0 \\ 0 & 0 \end{bmatrix}. \tag{10}$$

The common matrix of the system connects the output Jones vector, which describes the state of light polarization at the output of the optical circuit, with the input Jones

vector, which describes the state of light polarization at the input of the optical circuit, according to Eq. (11)

$$[D_{\text{out}}] = [T] \cdot [D_{\text{in}}]. \tag{11}$$

Then the intensity of the light beam is calculated like

$$I = \left[D^*_{out}\right]^T \cdot [D_{out}]. \tag{12}$$

Finally, the received intensity is transmitted to the signal processing unit.

3 Computer Simulation of the Fiber Optic Current Sensor

3.1 Building of the Fiber Optic Current Sensor Model in LabVIEW

As the FOCS prototype control and processing algorithms were implemented in LabVIEW programming environment the decision was made to develop a simulation model using the same tools. LabVIEW is a graphical programming language that uses graphical images (icons) as functions providing a perfect clarity and traceability of code logic. This made LabVIEW a widely adopted tool for solving various scientific and engineering tasks, including implementation of models of fiber-optic systems [11].

It provided us such advantages as mock-up's code reuse along with ability to add, exclude or replace various elements of the optical scheme without rewriting the program code. In addition, it is not always possible to conduct an analytical solving of the influence of parasitic factors. Prototype measurement error and analysis are significantly complicated by the presence of all disturbing factors simultaneously. In this regard, the proposed FOCS simulation allows to significantly simplify the analysis. It does not require to derivate the analytical formula, it is only needed to set parameters for the model, for example, the frequency and amplitude of the modulation, as well as to set parameters for external influences.

Each matrix in Eq. (10) was modeled as a separate virtual instrument (VI), storing in LabVIEW and being called in the common program for the FOCS model. Figure 2 shows the program code that forms the rotation matrix.

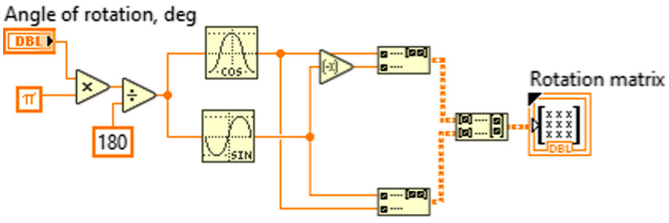

Fig. 2. Program code in LabVIEW for forming the rotation matrix.

Figure 3 shows a part of the common program for the FOCS model. It demonstrates the matrix of circuit elements as VI and their connection in the common program. The

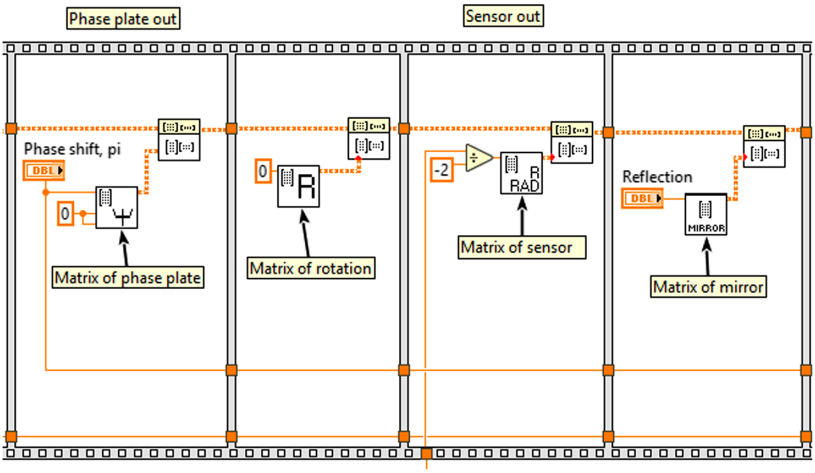

Fig. 3. FOCS modeling in LabVIEW (the part of block diagram).

advantages of this approach are visibility and the ability to add, exclude or replace various optical elements without rewriting the program code, because the matrices of each element are located in separate frames.

The FOCS model used additional phase modulation with a 40 kHz harmonic signal and digital phase detection based on the analysis method of the harmonics ratio of modulation frequency [8]. A harmonic signal with a frequency of 50 Hz was set as a signal simulating an electric current and acting on a sensitive fiber. Thus, the real-time FOCS model generated the raw interference signal that arises at the output of the sensor optical circuit when magnetic field is exposed to the sensor fiber, as well as demodulated signal that characterized this effect (see Fig. 4). This output signal set corresponds to the real laboratory prototype of the FOCS.

Based on Fig. 4, it can be seen that the demodulated signal is identical to the measured harmonic current signal with a frequency of 50 Hz. The developed model, implemented in LabVIEW, describes the actual physical processes occurring in the FOCS. The result of the simulation is fully confirmed by measurements of the FOCS laboratory prototype. In addition, the model can be used for debugging FOCS signal processing algorithms, since it is optimized for both floating-point and fixed-point values, which is necessary for implementing the code on the FPGA.

The FOCS measurement error and its analysis are substantially complicated by the presence of all external parasitic factors at the same time. In this regard, the developed FOCS model will simplify the study. For example, we can add noise to the system, polarizing mismatches at the junctions of fibers, take into account the imperfection of the quarter-wave plate and individually research the influence of each factor on the measurement accuracy.

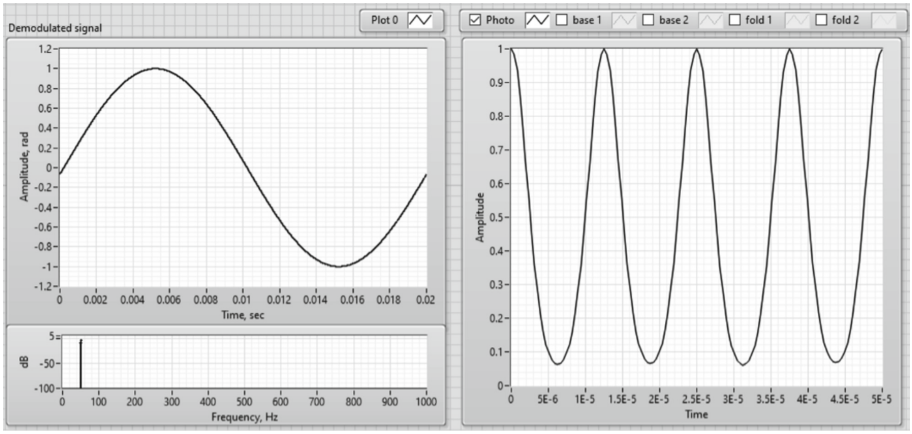

Fig. 4. Interference signal (on the right), demodulated signal and its spectrum (on the left), obtained during the FOCS modeling.

3.2 Influence of Polarization Mismatches on the Accuracy of Fiber Optic Current Sensor Measurements

The case of polarization mismatches occurrence in the circuit element located after modulator and before the sensitive element, namely at point 8 of the FOCS optical circuit, was investigated. For this purpose, we assume $\alpha_8 \neq 45°$ (see Fig. 1).

Using the developed model, the dependence of the measured current amplitude error and the total harmonic distortion on the angle of mismatch at point 8 was obtained (see Fig. 5). The demodulated signal and its spectrum in the ideal case and with polarization mismatch by 10° demonstrated on the Fig. 6.

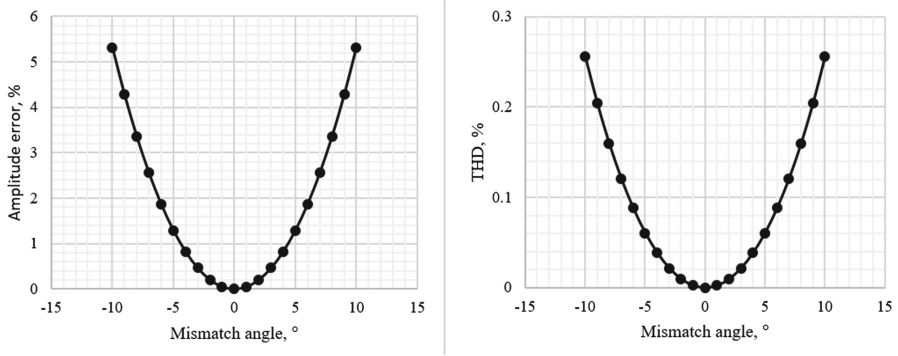

Fig. 5. Current amplitude error vs. Angle of polarization mismatch at point 8 (on the left). The total harmonic distortion vs. Angle of polarization mismatch at point 8 (on the right).

The research showed that the permissible tolerance of polarization mismatches at one of the optical circuit points located after the modulator and before the sensitive fiber

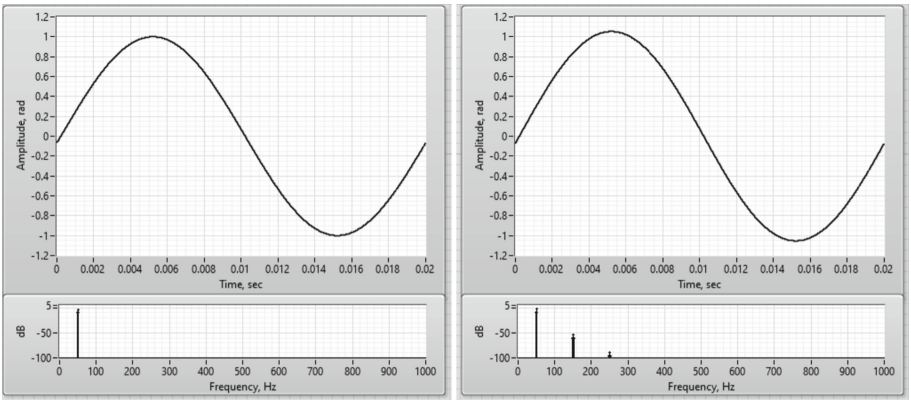

Fig. 6. Demodulated current signal and its spectrum. The angle of polarization mismatch at point 8 is 0° (on the left) and 10° (on the right).

is ±2° to achieve the FOCS accuracy class 0.2. In addition, the average level of the interference signal at the output of the optical circuit decreased by 9% with a mismatch angle of 10°.

3.3 Influence of Quarter-Wave Plate Imperfections on the Accuracy of Fiber Optic Current Sensor Measurements

The fiber quarter-wave plate is one of the most important elements of the FOCS optical circuit and the most difficult element in manufacturing. It is used to convert linearly polarized light modes into circularly polarized modes. This is necessary because the circularly polarized optical radiation is preserved in the sensitive spun fiber. In addition, when reflected from a mirror, modes with circular polarization change the direction of rotation to the opposite. Therefore, when the light passes back through the quarter-wave plate, the x-mode turns into the y-mode and vice versa. As a result, the sensor's current sensitivity is doubled.

A quarter-wave plate is a small piece of birefringent fiber only a few millimeters in size, but the accuracy of the entire huge system depends on it. Because of the research, it was found that the incorrect manufacturing of a quarter-wave plate, expressed in a mismatch in its length, leads to a significant increase in the current amplitude error and the appearance of nonlinear distortions (see Fig. 7 and Fig. 8).

In difference from the effect of polarization mismatches at the points of element junctions or fiber splicing, the quarter-wave plate also affects the contrast of the interference signal at the output of the optical circuit (see Fig. 9). The signal contrast was calculated using the equation

$$V = \frac{I_{max} - I_{min}}{I_{max} + I_{min}} \cdot 100\%, \tag{13}$$

where I is the signal intensity at the optical circuit output.

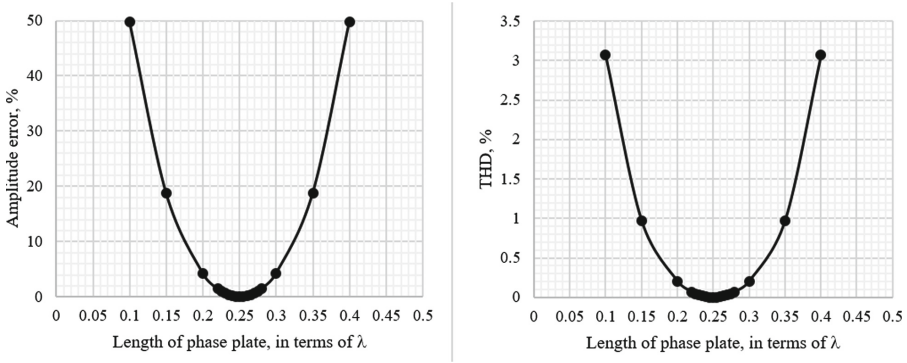

Fig. 7. Current amplitude error (on the left) and Total harmonic distortion (on the right) vs. length of phase plate.

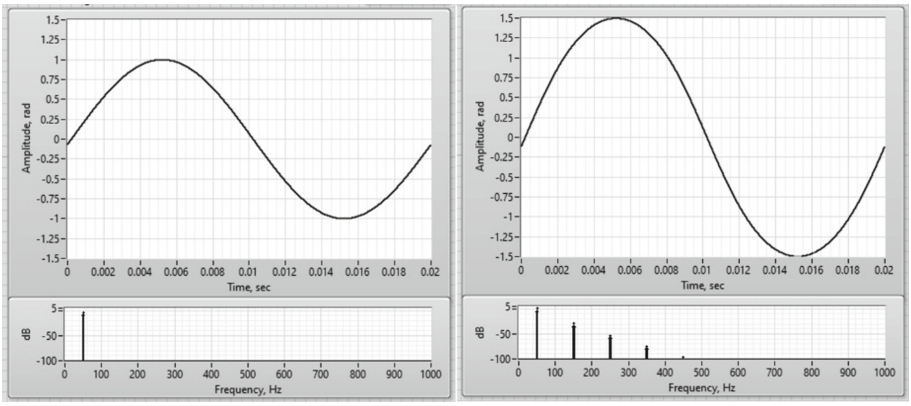

Fig. 8. Demodulated current signal and its spectrum in the case of ideal quarter-wave plate (on the left) and a phase plate with a length of 0.1λ (on the right).

This shows that imperfect quarter-wave plates reduce the signal contrast and thereby limit the dynamic range of the current sensor. It is due to the fact that modes with elliptical polarization are formed at the output of the phase plate. These modes are not converted to orthogonal modes when reflected from a mirror. As a result, when light passes back through the phase plate, the output is again elliptically polarized modes, rather than linear ones [7].

Thus, the permissible tolerance of the error of the quarter-wave plate length is ±0.01λ to achieve the FOCS accuracy class 0.2. In these error margins the contrast of the interference signal is reduced by only 0.62%.

A similar study was conducted with the FOCS mock-up. The results of the experiments coincided with the simulation results. It confirmed the efficiency of the developed model and the relevance of its application for finding ways to eliminate the overall FOCS errors.

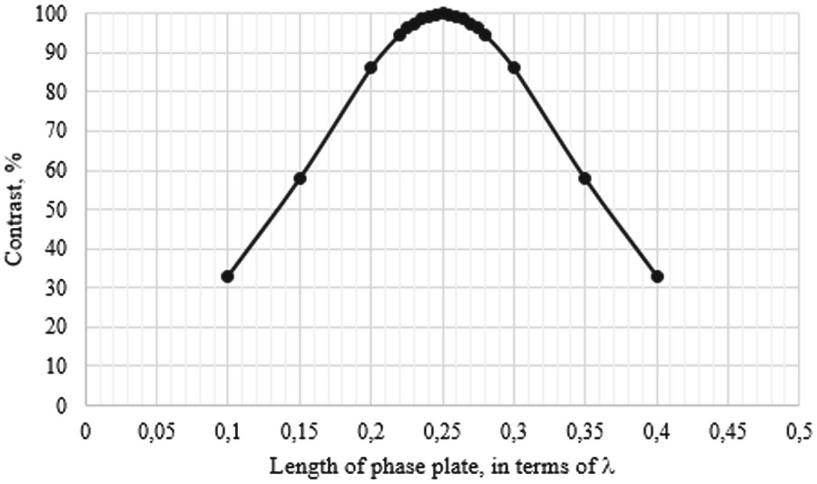

Fig. 9. Contrast of the interference signal vs. length of phase plate.

4 Conclusion

As a result of the research, the FOCS model was developed based on the Jones matrices formalism instead of physical object. Implementation of the model in the LabVIEW programming environment allowed us to study the sensor operation without analytical derivation of formulas. Experiments have shown that the developed model is a digital twin of the FOCS real prototype. The influence of polarizing mismatches in the places of fiber splicing or junctions between optical elements, as well as the incorrectness of manufacturing a quarter-wave plate on the accuracy of current sensor measurements was studied. When polarizing mismatches are introduced, the amplitude error of the current sensor and the non-linearity of the output signal increase. While the imperfection of the quarter-wave plate also affects the contrast of the interference signal at the optical circuit output, and therefore the dynamic range of the device. In order for the FOCS meets the accuracy class 0.2, it is necessary to ensure that the error of junctions between elements is not more than $\pm 2^\circ$ and the error of manufacturing a quarter-wave plate is not more than $\pm 0.01\lambda$. The results of the experiments with the real prototype coincided with the simulation results.

The other advantage of the developed model is the fact that the program code is optimized for implementation on the FPGA but with the benefits of high-level debugging tools. In addition thanks to the LabVIEW features the model appears extremely flexible and reconfigurable to implement alternative FOCS schemes, which allows us to explore the sensor in various configurations.

References

1. Ripka, P.: Electric current sensors: a review. Meas. Sci. Technol. **21**(11), 112001 (2010)
2. De Nazaré, F., Werneck, M.: Hybrid optoelectronic sensor for current and temperature monitoring in overhead transmission lines. IEEE Sens. J. **12**(5), 1193–1194 (2012)

3. Blake, J.N.: Fiber optic current sensor. Patent No. US 6,188,811 B1, Int. Cl. G02B 6/00, G01J 4/00, 13 February 2001
4. Bohnert, K., Gabus, P., Nehring, J., Brandle, H.: Temperature and vibration insensitive fiber-optic current sensor. J. Lightwave Technol. **20**(2), 267–276 (2002)
5. Boev, A., et al.: Fibre-optic current sensor. Patent RU 2437106 C2, G01R 15/24, G01R 19/2, 20 December 2011. Bull. 35
6. Bohnert, K., Hsu, C., Yang, L., Frank, A., Müller, G.M., Gabus, P.: Fiber-optic current sensor tolerant to imperfections of polarization-maintaining fiber connectors. J. Lightwave Technol. **36**(11), 2161–2165 (2002)
7. Przhiyalkovsky, Y., Morshnev, S., Starostin, N., Gubin, V.: Modified sensing element of a fibre-optic current sensor based on a low-eigenellipticity spun fibre. Quantum Electron. **44**(10), 957–964 (2014)
8. Temkina, V., Medvedev, A., Mayzel, A., Mokeev, A.: Fiber optic current meter for IIoT in power grid. In: Galinina, O., Andreev, S., Balandin, S., Koucheryavy, Y. (eds.) NEW2AN/ruSMART -2018. LNCS, vol. 11118, pp. 631–640. Springer, Cham (2018). https://doi.org/10.1007/978-3-030-01168-0_57
9. Temkina, V., Medvedev, A., Mayzel, A., Mokeev, A.: Compensation of fiber quarter-wave plate temperature deviation in fiber optic current sensor. In: 2019 IEEE International Conference on Electrical Engineering and Photonics (EExPolytech), pp. 339–341. IEEE, St. Petersburg (2019)
10. Bhandari, R.: Transpose symmetry of the Jones matrix and topological phases. Opt. Lett. **33**(8), 854–856 (2008)
11. Harun, S.W., Emami, S.D., Arof, H., Hajireza, P., Ahmad H.: LabVIEW applications for optical amplifier automated measurements, fiber-optic remote test and fiber sensor systems. In: De Asmundis, R. (ed.) Modeling, Programming and Simulations Using LabVIEW™ Software, pp. 201–236. InTech (2011)